

A Variational Time Series Feature Extractor for Action Prediction*

Maxime Chaveroche¹, Adrien Malaisé², Francis Colas², François Charpillat², Serena Ivaldi²

Abstract—We propose a Variational Time Series Feature Extractor (VTSFE), inspired by the VAE-DMP model of Chen et al. [1], to be used for action recognition and prediction. Our method is based on variational autoencoders. It improves VAE-DMP in that it has a better noise inference model, a simpler transition model constraining the acceleration in the trajectories of the latent space, and a tighter lower bound for the variational inference. We apply the method for classification and prediction of whole-body movements on a dataset with 7 tasks and 10 demonstrations per task, recorded with a wearable motion capture suit. The comparison with VAE and VAE-DMP suggests the better performance of our method for feature extraction. An open-source software implementation of each method with TensorFlow is also provided. In addition, a more detailed version of this work can be found in the indicated code repository. Although it was meant to, the VTSFE hasn't been tested for action prediction, due to a lack of time in the context of Maxime Chaveroche's Master thesis at INRIA.

I. INTRODUCTION

The problem of recognizing actions or activities has been widely addressed in the computer vision research community: it consists in the classification of a fully or partially observed action, typically observed through cameras or external motion capture [2]. In robotics, recognizing the human activity is paramount for enabling a proper interaction and providing assistance to the human: an assistive device or prosthetics could switch control modes depending on the current human activity (e.g., walking or sitting) [3], [4]; a mobile robot may adapt its navigation depending on the prediction of the human motion [5]. More generally, prediction is important to provide the robot with anticipation capabilities [6]. In collaborative robotics applications in manufacturing, such as in assembly lines, recognizing the current activity of the operator is necessary for ergonomics evaluations [7] and for the optimization of the robot actions.

However, there are two critical issues that prevent the direct application of existing techniques in such scenarios.

The first issue is the availability of external sensing devices (cameras or motion captures) that poses constraints on the application for many tasks and application scenarios. Wearable sensors, such as the Xsens MVN Link [8], are a valid alternative to motion capture and cameras: they offer the same tracking possibilities for the human kinematics and simplify the extraction of the body posture in case of

occlusions (e.g., large objects or environment hiding body parts) and long distances not necessarily covered by cameras.

The second issue is that the information about the current activity may be not enough for the robot to take appropriate decisions (e.g., in case of physical interaction), and it may be necessary to predict also the entire trajectory for the action. For example, a collaborative robot may need to predict the goal and trajectory of the human while carrying an object together [9] in order to generate appropriate coordinated actions [10]. This entails a prediction, classification and representation problem: we need to find a suitable representation of whole-body motions where the same features are used to recognize different actions and to predict the outcome of an action from early observations.

This presents two main challenges: i) extracting features of the action in time; ii) reducing the dimensionality of the problem to ease the prediction process, reduce overfitting and enable online applications. These challenges can be solved by the same process, provided that it builds a set of features that is smaller than the set of the input data dimensions, and that it contains both posture and dynamics features. In this paper, we focus on generative models for data sequences, as these techniques aim at building representations rich enough to generate plausible variants of that data.

Dynamic Bayesian Networks (DBN), such as *Hidden Markov Models* (HMM) and Kalman filters are often a simple and effective approach. For example, in [11] they were used for fall detection, to discriminate daily activities, such as walking and sitting, from falling or lying on the ground. HMM were also used in [12], to automatically identify meaningful low-dimensional feature vectors for motion recognition. However, these model-based approaches often rely on assumptions facilitating the inference but restricting their generality. We will thus focus on model-free approaches.

Some recent papers addressed the problem using *Deep Neural Networks* (DNN) trained on motion capture data. [13] used an encoder-recurrent-decoder model to predict motions. The encoder-decoder architecture learns to reconstruct postures, while the recurrent middle layer holds the temporal dynamics. In [1], Chen *et al.* proposed a generative model for human motion generation using a deep neural architecture with *Variational Inference* (VI) [14] and Bayesian filtering with *Dynamic Movement Primitives* (DMP) [15] which ensures local space-time continuity in movement representation in a reduced space. This latent space provides plausibility in data reconstruction, while being generalizable to new samples of movements.

In [16], the authors compared three different generative structures of encoder-decoder networks with temporal encod-

*This work was funded by the European Project An.Dy (no. 731540 H2020-ICT-2016-1) in the context of Maxime Chaveroche's Master thesis at INRIA in 2017.

¹ Université de Technologie de Compiègne (UTC), Heudiasyc (UMR CNRS 7253) name.surname@hds.utc.fr

² Inria Nancy - Grand Est, Team LARSEN name.surname@inria.fr

ing, enabling action prediction in the reduced feature space. Two used a fully connected DNN, while the last one used a *Convolutional Neural Networks* (CNN). In all these encoder-decoder networks, the encoder learns a smaller representation of an input subsequence $x_{t:t+S}$ while the decoder learns to predict the next data subsequence $x_{t+S+1:t+2S+1}$. These models slightly outperform the results in [13], have lower computational complexity once trained, and are therefore applicable to online tasks, but may overfit training data due to their deterministic mapping between subsequences.

[17] proposed a method for motion prediction that outperforms [13] by far, and is similar to [16], with the exception that a noise was applied to training samples, by feeding the network with its own generated predicted sequences. This noise injection at training time prevents the system overfitting. Nevertheless, the learned representation remains biased by the application, *i.e.* prediction, and thus might not learn useful features for recognition purposes. The same phenomenon may appear in [18], where a *Recurrent Neural Network* (RNN) was employed in a generative model, alongside *Variational Auto-Encoders* (VAE) [19], which generalizes features encoding while being biased by the integration of the RNN internal state variable.

To provide a more generalizable feature extraction, we propose a new generative model, called *Variational Time Series Feature Extractor* (VTSFE), which is task-independent since it is based on autoencoders. Our model is inspired by VAE-DMP [1] and further adds three improvements: i) a better noise inference model, described in Section III-A; ii) a simpler transition model based on a continuity constraint on the acceleration in the latent space, in contrast to the one in [1] represented by the DMP; iii) a tighter lower bound (*i.e.*, closer to $\ln(p_\theta(x_{1:T}))$) for the variational inference, as described in Section III-C. We discuss limits and benefits of the proposed method and show the results on prediction of whole-body movements using our open-source dataset of actions recorded with a wearable IMUs suit (Xsens MVN).

The paper is organized as follows. Section II introduces the related works at the base of VTSFE, described in detail in Section III. Sections IV and V describe the materials and the experiments with the wearable sensors. In Section VI and VIII we discuss our results, conclusions and outline future works.

II. RELATED WORKS AND METHODS

Our proposed method is inspired by the work of Chen et al. [1], which proposed a method called *Dynamic Movement Primitives in Latent Space of Time-Dependent Variational Autoencoders* (VAE-DMP). VAE-DMP is based on *Deep Variational Bayes Filters* (DVBF) [20] that integrate Bayesian filtering into a Recurrent Deep Neural Network made of chained *Variational Auto-Encoders* (VAE) [19]. VAEs build a feature space designed to generalize postures through a reduced set of latent variables, while Bayesian filtering ensures that time is taken into account into the spatial compression. In [1], that filtering appears in the

form of a *Dynamic Movement Primitives* (DMP), a trajectory/dynamics model usually employed in robotics for synthesizing movement primitives [15].

In the following, we will briefly overview the three key elements of [1], namely DMP, VAE, DVBF, that are also the key methods at the base of our proposed method VTSFE .

A. DMP

Dynamic Movement Primitives are a classical technique for learning movement primitives from demonstrated trajectories [15]. A DMP is a point attractor system written as a second-order dynamic model, aiming at representing a trajectory: $\tau\ddot{p}(t) = \alpha(\beta(p_{goal} - p(t)) - \dot{p}(t)) + f$, where p is the position, function of time, p_{goal} is the goal of the trajectory, and f represents the forcing term that captures the movement dynamics, τ is a time scaling term, α and β are constant values to tune.

B. VAE

A VAE [19] is an auto-encoder based on variational inference [14] that attempts to find a reduced representation of data generalizable to variants of that data.

Let $[x_k]_{k=1}^K$ be a dataset of K i.i.d. samples of some continuous observation variable x of unknown distribution. We assume that the data are generated by some random process, involving a latent continuous random variable z and parametric families of distributions $p_\theta(x|z)$ and $p_\theta(z)$: $x \sim \int_z p_{\theta^*}(x|z)p_{\theta^*}(z)dz$, where θ^* is the set of parameters of the parametric distribution $p_{\theta^*}(x)$. θ is represented by weights and biases of a *decoder* neural network. z is a latent space that can be chosen arbitrarily; in VAE, the distributions are chosen to be Gaussian for simplicity: $p_\theta(z) = \mathcal{N}(0, I)$ and $p_\theta(x|z) = \mathcal{N}(\mu_x, \sigma_x^2 I)$.

However, we don't know the distribution of $p_\theta(x)$, and so the distribution of $p_\theta(z|x)$ as $p_\theta(z|x) = \frac{p_\theta(z,x)}{p_\theta(x)}$. Therefore, [19] introduced a recognition model $q_\phi(z|x)$ designed to approximate the intractable true posterior $p_\theta(z|x)$. We could then constrain $q_\phi(z|x)$ to the same form as $p_\theta(x|z)$:

$$q_\phi(z|x) = \mathcal{N}(\mu_z, \sigma_z^2 I), \quad (1)$$

where ϕ is the set of parameters of the parametric distribution $q_\phi(z|x)$. ϕ is represented by weights and biases of an *encoder* neural network. This model can then simultaneously encode and decode x . Yet, we have to learn θ and ϕ in a way that maximizes the likelihood of $[x_k]_{k=1}^K$.

Training in VAE aims both at recovering parameters θ as close as possible to the ideal parameters θ^* yielding the proper distribution over x , and finding parameters ϕ making $q_\phi(z|x)$ as close as possible to the intractable $p_\theta(z|x)$. The latter can be achieved by minimizing the Kullback-Leibler divergence $D_{KL}(q_\phi(z|x) \parallel p_\theta(z|x))$ between these distributions. The standard approach of variational inference is to notice that we could decompose $\ln(p_\theta([x_k]_{k=1}^K))$, isolate $D_{KL}(q_\phi(z|x_k) \parallel p_\theta(z|x_k))$ and minimize it by maximizing a lower bound on $\ln(p_\theta(x_k))$:

$$\ln(p_\theta(x_k)) = ELBO + D_{KL}(q_\phi(z|x_k) \parallel p_\theta(z|x_k)) \quad (2)$$

where *ELBO* is the Evidence Lower Bound.

As the actual likelihood on the observation $p_{\theta^*}(x_k)$ is a constant and a KL-divergence is always non-negative, minimizing that KL-divergence can be done by maximizing the *ELBO*. In terms of training the neural network, it means using $-ELBO$ as the loss function to be minimized. This bound can in turn be split into respectively a *reconstruction* (or decoder) error and a *generalization* (or encoder) error:

$$-ELBO = -\mathbb{E}_{q_\phi(z|x_k)}[\ln(p_\theta(x_k|z))] + D_{KL}(q_\phi(z|x_k) \parallel p_\theta(z)) \quad (3)$$

The first term of this error requires precision in reconstruction from the network by making it maximize the average likelihood $p_\theta(x_k|z)$ on z inferred by the recognition model $q_\phi(z|x_k)$. The second term of this error requires generalization from the network and balances the first error which could result in overfitting otherwise. The difference between VAE and a deterministic auto-encoder comes from the influence of σ_z in the generalization term as it allows for the learning of a locally symmetrical and continuous latent space.

C. DVBF

Let us consider a set of data sequences $[[x_{k,t}]_{t=1}^T]_{k=1}^K$. In the following, we consider a single sample k and use only the notation \cdot_t , as we are mostly interested in time here.

DVBF [20] was introduced to handle time-dependency in data sequences. Latent variables are supposed to follow a dynamics equation expressed as:

$$z_{t+1} = g(z_t, u_t, \beta_t). \quad (4)$$

where g is a deterministic transition function, u_t is a given command at time t and β_t is a set of parameters written as $\beta_t = (w_t, v_t)$, where v_t are fixed universal transition parameters, and w_t is a stochastic variable representing a sample-specific process noise which can be inferred from x_t . In [20], the authors compute a variational lower bound specific to DVBF:

$$p_\theta(x_{1:T}|u_{1:T}, z_1) = \int_{\beta_{1:T}} p_\theta(\beta_{1:T}) p_\theta(x_t|z_1) \prod_{t=2}^T p_\theta(x_t|\hat{z}_t) d\beta_{1:T} \quad (5)$$

where $\hat{z}_t = g(z_{t-1}, u_{t-1}, \beta_{t-1})$. Then, taking the log of $p_\theta(x_{1:T}|u_{1:T}, z_1)$ and using Jensen's inequality, they obtain:

$$\begin{aligned} & \ln(p_\theta(x_{1:T}|u_{1:T}, z_1)) \\ & \geq \mathbb{E}_{q_\phi(\beta_{1:T}|x_{1:T}, u_{1:T}, z_1, \hat{z}_{2:T})} \left[\ln \left(p_\theta(x_t|z_1) \prod_{t=2}^T p_\theta(x_t|\hat{z}_t) \right) \right] \\ & \quad - D_{KL}(q_\phi(\beta_{1:T}|x_{1:T}, u_{1:T}, z_1, \hat{z}_{2:T}) \parallel p_\theta(\beta_{1:T})) \end{aligned} \quad (6)$$

This lower bound does not link to the minimization of $D_{KL}(q_\phi(z|x) \parallel p_\theta(z|x))$, but is a way to maximize the likelihood of $p_\theta(x_{1:T}|u_{1:T}, z_1)$, embedding transition parameters learning in the encoding process of the VAE.

D. VAE-DMP

In [1], Chen et al. used DMP as a dynamics model of the latent space in DVBF. They included a system noise $\epsilon_t = \epsilon w_{\epsilon,t}$, where $\epsilon \sim \mathcal{N}(0, \Sigma_\epsilon)$, in the DMP equation and defined their choice of finite difference approximations of first and second order derivatives:

$$\begin{cases} \tau \ddot{z}_{t+1} = \alpha(\beta(z_T - z_t) - \dot{z}_t) + f_t + \epsilon_t \\ \dot{z}_{t+1} = \ddot{z}_{t+1} dt + \dot{z}_t \\ z_{t+1} = \dot{z}_{t+1} dt + z_t, \end{cases} \quad (7)$$

where f_t is a continuous weighted sum of Gaussians and is deterministically inferred by a Multi-Layer Perceptron (MLP) detailed in [1] that takes $x_{1:T}$ as input. This system of equations can be reshaped into the following linear form:

$$\begin{pmatrix} z_{t+1} \\ \dot{z}_{t+1} \end{pmatrix} = \begin{pmatrix} 1 - dt^2 \alpha \beta \frac{1}{\tau} & dt^2 \alpha \frac{1}{\tau} + dt \\ -\alpha \beta dt \frac{1}{\tau} & 1 - \alpha dt \frac{1}{\tau} \end{pmatrix} \begin{pmatrix} z_t \\ \dot{z}_t \end{pmatrix} + b \quad (8)$$

with $b = (dt, 1)^\top (\alpha \beta z_T + f_t + \epsilon_t) dt \frac{1}{\tau}$.

Contrary to standard VAE, in VAE-DMP z_t is inferred by the dynamics model, along with its first-order derivative \dot{z}_t , at the exception of the first frame, which has no predecessor, and the last frame which is needed in Eq. 8. Therefore, the encoding process $q_\phi(z_1, \dot{z}_1|x_{1:M})$, where $1 < M \leq T$, is used for the first frame, and the standard one $q_\phi(z_T|x_T)$ is used for the last frame of the architecture. The noise is assumed inferred by a Gaussian distribution: $\epsilon_t \sim q_\phi(\epsilon_t|x_{t+1}, z_t) = \mathcal{N}(\mu_{\epsilon,t}, \Sigma_{\epsilon,t})$.

Eq. 8 in VAE-DMP replaces Eq. 4 of DVBF: z_t is now (z_t, \dot{z}_t) , the command u_t of DVBF is now the joint distribution of the forcing term and the goal in latent space (f_t, z_T) , and the transition parameters β_t the noise ϵ_t :

$$z_{t+1} = g(z_t, \dot{z}_t, z_T, f_t, \epsilon_t). \quad (9)$$

As $f_{1:T}$ are deterministically inferred from $x_{1:T}$, the variational lower bound becomes:

$$\begin{aligned} & \ln(p_\theta(x_{1:T}|f_{1:T}, z_T, z_1, \dot{z}_1)) \\ & \geq \mathbb{E}_{q_\phi(\epsilon_{1:T}|x_{1:T}, z_T, z_1, \dot{z}_1, \hat{z}_{2:T}, \hat{\dot{z}}_{2:T})} [\ln(p_\theta(x_1|z_1)p_\theta(x_{2:T}|\hat{z}_{2:T}))] \\ & \quad - D_{KL}(q_\phi(\epsilon_{1:T}|x_{1:T}, z_T, z_1, \dot{z}_1, \hat{z}_{2:T}, \hat{\dot{z}}_{2:T}) \parallel p_\theta(\epsilon_{1:T})) \end{aligned} \quad (10)$$

where we call the lower bound $ELBO_{VAE-DMP}$ and $q_\phi(\epsilon_{1:T}|x_{1:T}, z_T, z_1, \dot{z}_1, \hat{z}_{2:T}, \hat{\dot{z}}_{2:T}) = q_\phi(\epsilon_{1:T}|x_{1:T}, z_1, \hat{z}_{2:T})$ given their inference model.

We note that the parameters of the prior $p_\theta(\epsilon_t)$ are not fixed values in [1], which lets the D_{KL} calculation unclear, since its regularization power relies on fixed constraints.

III. PROPOSED METHOD: VTSFE

In this section we describe our Variational Time Series Feature Extractor (VTSFE) for action prediction. The model, inspired by VAE-DMP, is shown in Figure 1 and has three distinguishing features: *i*) it has a better noise inference model, described in Section III-A; *ii*) the transition model, that in [1] is represented by the DMP, here is substituted by a simple continuity constraint on the acceleration in the latent space, as described in Section III-B; *iii*) it has a tighter

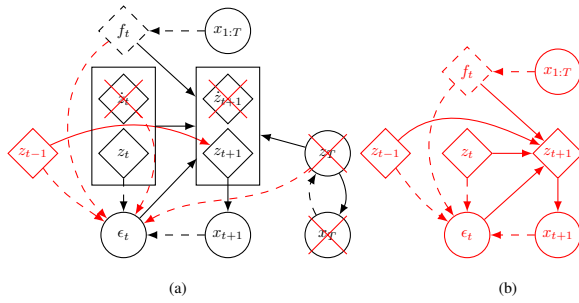


Fig. 1. Our VTSFE representation consisting of the superposition of two Bayesian models (a) compared with VAE-DMP, (b) alone. The black part is the VAE-DMP model from [1], the red arrows indicate our added dependencies. Red nodes and red crosses indicate respectively added variables and removed variables in our final model (b). Dependencies to θ and ϕ have been omitted for the sake of clarity. Solid lines denote the generative model with parameters θ , dashed lines denote the inference model with parameters ϕ . Diamond nodes indicate a deterministic dependency on parent nodes. Diamond dashed node indicates a deterministic dependency on parent nodes for the inference model but not the generative one. A rectangle designates the joint distribution of the variables inside, here (z_t, \dot{z}_t) .

lower bound (i.e., closer to $\ln(p_\theta(x_{1:T}))$) for the variational inference, as described in Section III-C.¹

A. Adapted noise inference

VAE-DMP uses the inference model of DVBF. However, the change of variable between z_t and (z_t, \dot{z}_t) and the dependency on z_T of the transition model should affect the noise inference, which is supposed to fill the gap remaining between information contained in the latent space and the one in observation space. Besides, knowing x_{t+1} alone isn't enough to deterministically infer f_t . Therefore, we propose the new following noise inference: $\epsilon_t \sim q_\phi(\epsilon_t | f_t, x_{t+1}, z_t, \dot{z}_t, z_T)$, if one chooses to use \dot{z}_t , or: $\epsilon_t \sim q_\phi(\epsilon_t | f_t, x_{t+1}, z_t, z_{t-1}, z_T)$, otherwise. The corresponding Bayesian models are illustrated in Figure 1.

Now, let us assume that the prior $p_\theta(\epsilon_t)$ of our model is a Gaussian white noise that does not depend on t . We consider σ_{scale} the scaling term for all noise ϵ_t , that also affects its inference mean knowing x_t . We could then make the following assumptions:

$$\begin{aligned} q_\phi(\epsilon_t | f_t, x_{t+1}, z_t, z_{t-1}, z_T) &= \mathcal{N}(\sigma_{scale} \cdot \mu_{\epsilon,t}, \sigma_{scale}^2 \sigma_{\epsilon,t}^2 I) \\ p_\theta(\epsilon_t) &= \mathcal{N}(0, \sigma_{scale}^2 I). \end{aligned} \quad (11)$$

Actually, as $\mu_{\epsilon,t}$, σ_{scale} and $\sigma_{\epsilon,t}$ are all inferred by our neural network, this formulation is equivalent to:

$$\begin{aligned} q_\phi(\epsilon_t | f_t, x_{t+1}, z_t, z_{t-1}, z_T) &= \mathcal{N}(\mu_{\epsilon,t}, \sigma_{\epsilon,t}^2 I) \\ p_\theta(\epsilon_t) &= \mathcal{N}(0, \sigma_{scale}^2 I), \end{aligned} \quad (12)$$

but leads to a lighter Kullback-Leibler divergence expression.

¹Supplementary material regarding some computations (not reported for lack of space) can be found at: <https://github.com/inria-larsen/activity-recognition-prediction-wearable/tree/master/VTSFE>

B. Lighter transition model

In [1] DMPs were used as a space-time continuity constraint, i.e., a constraint that gives to the network the notion of continuous acceleration. However, we would like to remove the dependency to the point-attractor aspect of DMP, remove the hyperparameters α , β and τ , as well as the appearance of z_T in its equation. Thus, in association with the central finite difference approximator of acceleration (which is more accurate than the backward and forward variants), Eq. 7 simply becomes:

$$\begin{cases} \ddot{z}_t = f_t + \epsilon_t \\ \ddot{z}_t = \frac{z_{t+1} - 2z_t + z_{t-1}}{dt^2} \end{cases} \quad (13)$$

Eq. 8 then becomes: $z_{t+1} = (f_t + \epsilon_t)dt^2 + 2z_t - z_{t-1}$, where dt doesn't even act as a hyperparameter neither since f_t and ϵ_t are learned and completely artificial. The new transition models, formerly Eq. 9, becomes: $z_{t+1} = g(z_t, z_{t-1}, f_t, \epsilon_t)$ and it has several benefits. First, it removes the model parametrization, which prevents us from doing an expensive grid search. Then, it greatly alleviates the complexity of our model both at transition time and at loss computation time, since it removes the need to sample the z_T prior.

C. Lower bound

In this subsection, we will define a new lower bound for our VTSFE model to use as loss function. We will make the calculation with the full DMP transition model to obtain a general lower bound, whether we use the point-attractor aspect or not. Contrary to [1], we will not use the DVBF lower bound, as the main difference in VTSFE and VAE-DMP with respect to DVBF is that unknown forcing term f_t replace observed commands u_t . This means that we could look for a different variational lower bound using $\ln(p_\theta(x_{1:T}))$ rather than $\ln(p_\theta(x_{1:T} | f_{1:T}, z_T, z_1, \dot{z}_1))$ as in Eq. 10. Similarly to Eq. 22, we can write:

$$\begin{aligned} ELBO &= \mathbb{E}_{q_\phi(z_{1:T} | x_{1:T})} [\ln(p_\theta(x_{1:T} | z_{1:T}))] \\ &\quad - D_{KL}(q_\phi(z_{1:T} | x_{1:T}) \parallel p_\theta(z_{1:T})) \end{aligned} \quad (14)$$

Instead of inserting the derivative in the state so as to get a first-order Markov assumption, we simply use the second-order Markov property. With a VAE encoder only for the first, second and last time steps, we can show that:

$$\begin{aligned} &\mathbb{E}_{q_\phi(z_{1:T} | x_{1:T})} [\ln(p_\theta(x_{1:T} | z_{1:T}))] \\ &= \sum_{t \in \{1, 2, T\}} \mathbb{E}_{q_\phi(z_t | x_t)} [\ln(p_\theta(x_t | z_t))] \\ &\quad + \sum_{t=3}^{T-1} \mathbb{E}_{q_\phi(z_{1:t}, z_T | x_{1:T})} [\ln(p_\theta(x_t | z_t))], \end{aligned} \quad (15)$$

and:

$$\begin{aligned} &D_{KL}(q_\phi(z_{1:T} | x_{1:T}) \parallel p_\theta(z_{1:T})) \\ &= \sum_{t \in \{1, 2, T\}} D_{KL}(q_\phi(z_t | x_t) \parallel p_\theta(z_t)) \\ &\quad + \sum_{t=2}^{T-2} \mathbb{E}_{q_\phi(z_{1:t}, z_T | x_{1:T})} \left[-\ln(p_\theta(\hat{f}_t)) \right. \\ &\quad \left. + D_{KL}(q_\phi(\epsilon_t | \hat{f}_t, x_{t+1}, z_t, z_{t-1}, z_T) \parallel p_\theta(\epsilon_t)) \right], \end{aligned} \quad (16)$$

where \hat{f}_t is the deterministic inferred value of f_t for a given $x_{1:T}$. Then, following [21] and using Eq. 11,

we get: $D_{KL}(q_\phi(\epsilon_t|f_t, x_{t+1}, z_t, z_{t-1}, z_T) \parallel p_\theta(\epsilon_t)) = \frac{1}{2} \sum_{i=1}^{d_z} [-\ln(\sigma_{\epsilon_t, i}^2) - 1 + \sigma_{\epsilon_t, i}^2 + \mu_{\epsilon_t, i}^2]$.

Using the same discrete approximation of the mean as in [19], this leads us to a computationally highly expensive approximation in $\Theta(L^{T-3})$. In order to be able to compute that new lower bound, we made a rougher approximation by taking the L^3 samples from the three priors $p_\theta(z_1)$, $p_\theta(z_2)$ and $p_\theta(z_T)$, and for all $t \in [2, T-2]$, only propagating $z_{t+1} = g(\mu_{z, T}, \mu_{z, t}, \mu_{z, t-1}, \mu_{\epsilon_t}, \hat{f}_t)$ for each of these L^3 3-tuples $(z_{l_1}, z_{l_2}, z_{l_T})$, which changes Eq. 11 to:

$$\begin{aligned} & q_\phi(\epsilon_t|f_t, x_{t+1}, z_t, z_{t-1}, z_T) \\ &= \mathcal{N}\left(\sigma_{scale} \cdot \mu_{\epsilon_t}, \sigma_{scale}^2 \left(\sigma_{\epsilon_t}^2 + K^2 \sum_{t'=2}^{t-1} \sigma_{\epsilon_{t'}}^2\right) I\right) \\ & p_\theta(\epsilon_t) = \mathcal{N}(0, [1 + (t-2)K^2] \sigma_{scale}^2 I) \end{aligned} \quad (17)$$

as g is a linear transformation. K is the real factor that multiplies ϵ_t in g . Thereby, we obtain that $D_{KL}(q_\phi(\epsilon_t|f_t, x_{t+1}, z_t, z_{t-1}, z_T) \parallel p_\theta(\epsilon_t))$ leads to $\sum_{t=2}^{T-2} L^3$ samples and thus a $\Theta(L^3)$ complexity to approximate the expectation of D_{KL} . That approximation has also been used on Eq. 31 with 4-tuples $(z_{l_1}, z_{l_2}, z_{l_t}, z_{l_T})$ instead of the previous 3-tuples in order to sample the latent space at each inference on z as in VAE, leading to $\Theta(L^4)$.

Also concerning Eq. 31, it is worth mentioning that $\sigma_{x, t}$ is only used in the reconstruction loss term, without any other constraint. Therefore, it acts as a degree of freedom at optimization time that can compensate errors either by being high to reduce the squared error or by being very close to zero to make the log take a negative value if the error is small, which in particular could happen if the input data range doesn't vary much around zero, as it is the case for our data that ranges in $[-1, 1]$. Besides, having a different $\sigma_{x, t}$ for each z sample causes the optimization process to treat each error differently which reinforces these issues. Thus, in order to correct that error compensation and to save gradient computations, we made an additional assumption on $p_\theta(x_t|z_t)$ by setting $\sigma_{x, t}^2 = \frac{1}{2\pi}$, where the value $\frac{1}{2\pi}$ has been chosen to remove all constant term so the reconstruction error is entirely due to the squared term. This new assumption allows us to replace the expression of $\ln(p_\theta(x_t|z_t))$ with:

$$\ln(p_\theta(x_t|z_t)) = \pi(x_{t, i} - \mu_{x, t, i})^2 \quad (18)$$

Let us now define the last term of our lower bound. Unfortunately, $p_\theta(\hat{f}_t)$ is intractable. We could simply continue without it though, giving us a lower bound of $D_{KL}(q_\phi(z_{1:T}|x_{1:T}) \parallel p_\theta(z_{1:T}))$. Nevertheless, considering it as an important loss term on dynamics reconstruction, we want to keep at least a part of it. We notice that, being the result of a Kullback-Leibler divergence with a Dirac distribution, it acts as a penalty if $P_\theta(\hat{f}_t) \neq 1$. However, given the fact that without any knowledge, f_t could be equally anything, as x_t , $p_\theta(f_t)$ should be closer to a uniform distribution over an infinite space than a Dirac distribution centered on a particular \hat{f} . Thus, we assume that $-\mathbb{E}_{q_\phi(z_{1:T}|x_{1:T})}[\ln(p_\theta(\hat{f}_t))] \geq -\mathbb{E}_{q_\phi(z_{1:T}|x_{1:T})}[\ln(p_\theta(\hat{f}_t|z_{1:T}))] \geq 0$ since \hat{f}_t is used to

infer $z_{1:T}$. So we need to define $p_\theta(f_t|z_{1:T})$. First, we make the assumption that it follows a Gaussian distribution. Then, given the deterministic transition function $z_{t+1} = g(z_{l_T}, z_t, z_{t-1}, \epsilon_t, f_t)$, where ϵ_t is simply added to f_t , we notice that the only variance contained in $p_\theta(f_t|z_{1:T})$ is the one of $p_\theta(\epsilon_t)$. Besides:

$$\begin{aligned} p_\theta(f_t|z_{1:T}) &= \int_{x_{1:T}} p_\theta(f_t|x_{1:T}, z_{1:T}) p_\theta(x_{1:T}|z_{1:T}) dx_{1:T} \\ &\approx \int_{x_{1:T}} q_\phi(f_t|x_{1:T}) p_\theta(x_{1:T}|z_{1:T}) dx_{1:T}. \end{aligned} \quad (19)$$

Thereby, we make the assumption that $p_\theta(f_t|z_{1:T}) \approx \mathcal{N}(d(x_{1:T}), [1 + (t-2)K^2] \sigma_{scale}^2 I)$, where $x_{1:T} \sim p_\theta(x_{1:T}|z_{1:T})$ and d represents a function taking $x_{1:T}$ as input and $f_{1:T}$ as output where $f_{1:T} \sim q_\phi(f_t|x_{1:T})$, as the MLP used to infer $f_{1:T}$.

Unfortunately, even combined with the previously defined $\Theta(L^3)$ approximation of $\mathbb{E}_{q_\phi(z_{1:T}|x_{1:T})}$, the additional sampling on $x_{1:T}$ still leads to a $\Theta(L^3 \times X^T)$ approximation, where X is the number of samples taken for x_t . Therefore, we made an even rougher approximation by taking $X = 1$, where that only sample is the T-tuple $(\mu_{x, t})_{t \in [1:T]}$ and $\mu_{x, t}$ is the mean of $p_\theta(x_t|z_t)$.

Finally, we obtain the following relations on the various Evidence Lower BOunds (*ELBO*):

$$ELBO \geq ELBO_{VTSFE} \geq ELBO_{VAE-DMP}$$

More precise mean approximations aside, our lower bound $ELBO_{VTSFE}$ is thereby tighter to the initial *ELBO* than the DVBF one from which derives $ELBO_{VAE-DMP}$ thanks to our *dynamics reconstruction loss term* $-\mathbb{E}_{q_\phi(z_{1:T}|x_{1:T})}[\ln(p_\theta(\hat{f}_t|z_{1:T}))]$.

However, due to our approximations, we end up with a complexity, given T , of $\Theta(L^4)$ (or more precisely of $\Theta(P^3 \times M)$, where P is the number of samples from each of the priors $(z_{l_1}, z_{l_2}, z_{l_T})$ to propagate through time, and M is the number of samples from ϵ_{t-1} at time t).

That new lower bound is more computationally expensive, but should allow the creation of a more generalizable latent space by creating local space continuity in terms of both surroundings of each input and trajectory of the whole sequence, i.e. reducing the intraclass variance in latent space for each movement type, for L^3 trajectory initialization samples (prior sampling). At the same time, it forces the reconstructed inputs $x_{1:T}$ to keep the same dynamics as the actual inputs, in addition to force them to be individually close to the actual ones.

To reduce the complexity, we propose a *light VTSFE* by making a rough $\Theta(L)$ approximation consisting of only one prior sampling $(\mu_{z, 1}, \mu_{z, 2}, \mu_{z, T})$ for D_{KL} and only L samples $(\mu_{z, 1}, \mu_{z, 2}, \mu_{z, T}, z_{l_t})$ for $-\mathbb{E}_{q_\phi(z_{1:T}|x_{1:T})}[\ln(p_\theta(x_t|z_t))]$. This version reduces intraclass variance in latent space for each movement type, but only processes one trajectory initialization sample (prior sampling).

D. Neural network architecture

1) *Differences with respect to the original VAE*: We used a Gaussian MLP (as defined in appendix C of [19]) as encoder to model $q_\phi(z|x)$, and another Gaussian MLP as decoder to model $p_\theta(x|z)$. Instead of *tanh* as activation function for hidden layers, we used *elu* (Exponential Linear Unit) [22], as it outperforms state-of-the-art activation functions in learning speed and accuracy, and alleviates the vanishing gradient problem. We used the ADAM optimization algorithm [23] instead of ADAGRAD [24].

2) *Sequence architecture*: Since we want to build a unique latent space for all movement frames, all network variables are shared between time steps. As in [1], because of the vanishing gradient problem and the lack of movement demonstrations (but mostly because we want the original VAE to process all inputs and only use the DMP equation as a constraint), we split our samples into overlapping subsequences of size l_{sub} , where the architecture of our neural network is built using $T = l_{sub}$. The overlap is equal to $l_{sub} - n_V$, where n_V is the number of standard VAEs. However, we used the whole data sequence to infer $f_{1:T}$ given $x_{1:T}$ in order to remove a degree of freedom at optimization time between subsequences; we used *elu* instead of *softmax* as activation function in the MLP that infers $f_{1:T}$ for the same reasons than above.

E. Loss function gradients

Learning occurs through the back-propagation algorithm given a loss function and its gradients. To ensure precision, all gradient computations were made atomically, i.e. per time step and per dimension, but the back-propagation algorithm always was executed per subsequence. There are several ways to compute these gradients: simply computing the gradients from the whole loss function, computing them from subparts of that loss function, computing gradients for only a subset of variables, etc. Here, we considered two main learning schemes for the VTSFE learning. The first, called “*all*”, simply computes gradients for all variables from the whole loss function. It was applied to the chain of independent VAEs. The second, called “*separated*”, was applied to VTSFE and our implementation of VAE-DMP. First, *separated* computes gradients for all variables from the recognition loss term, as it takes account for the whole system leading to the reconstruction of x_t . Then, it computes gradients from the generalization loss term for only encoder variables on which it depends. i.e. not σ_{scale} . Finally, it computes gradients from the dynamics loss term for a subset of variables composed of all variables except the weights that define the forcing term f_t and the noise scaling variable σ_{scale} , since the dynamics loss term is supposed to only influence the quality of the decoder and, as a side effect, the one of the ϵ_t encoder; It should not try to optimize directly the variables used to compute its loss, i.e. Gaussian basis weights defining f_t and σ_{scale} , to avoid optimization shortcuts.

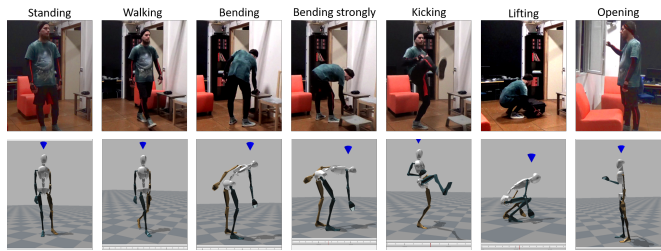


Fig. 2. Top: the actions of our dataset (we have 10 demonstrations per action). Bottom: the kinematics estimation of the human posture during the actions, in Xsens MVN studio.

IV. MATERIALS

1) *Equipment*: To capture human motion, we use an Xsens MVN inertial motion capture suit [8], a wearable system with 17 wireless IMUs embedded in a lycra suit, tracking motion at 240Hz. IMUs data are mapped on a calibrated Xsens biomechanical model with 23 segments, connected via 22 three-dimensional joints. Our sequences thereby have 66 dimensions.

2) *Dataset*: To compare our VAE-DMP implementation with the original, we retrieved from the authors of [1] their dataset. It consisted of 5 sample trajectories, one per movement type (kicking, tachi, balancing, walking, punching), consisting of body joint angles recorded from a motion capture system. To develop our model, we recorded a new dataset with our wearable sensing suit. Our dataset is made of 10 demonstrations per 7 movement types, of about 2 seconds. These movements were chosen for either their similarity with each others, their complexity (the more the limbs are in movement, the more difficult it is to make compromises in a representation common to several movement) and/or their relevance in the context of industrial scenarios. These movements are: bent forward to move an object, strongly bent forward, lifting a box from the ground, kicking, opening a window, walking and standing (see Figure 2).

3) *Software*: Our software and dataset are open-source and available on github at: <https://github.com/inria-larsen/activity-recognition-prediction-wearable>.

V. EXPERIMENTS

We consider the following four models:

- I Our $\Theta(L^3)$ VTSFE model, with tighter lower bound and no attractor point,
- II A $\Theta(L)$ light variant of (I), which only considers the trajectory resulting from one single sample from the z priors, i.e. $(\mu_{z,1}, \mu_{z,2})$,
- III Our $\Theta(L)$ implementation of [1] ²,
- IV Independent standard VAEs trained with overlapping subsequences.

²We use their lower bound on the trajectory composed of $(\mu_z, \mu_{\dot{z}})_{1:T}$ with the DMP attractor point system and without the dynamics reconstruction loss term, our $p_\theta(\epsilon_t)$, our Gaussian log likelihood without variance (Eq. 18), their noise inference model and without their annealing schedule described in [1], since our additional assumptions and implementation resolved the problem of ϵ_t acting as a shortcut to encode dynamics information.

	MSE $\times 10^{-3}$	$\sum var$
VTSFE light (II) 2D	10.195466	≈ 10
VAE-DMP (III) 2D	9.2731696	≈ 5
VAE only (IV) 2D	8.0171376	≈ 5.5
VTSFE light (II) 5D	9.8597025	≈ 9.5
VAE-DMP (III) 5D	8.5839415	≈ 3.5
VAE only (IV) 5D	8.3727958	≈ 6
VTSFE light (II) 7D	9.835138	≈ 9.5
VAE-DMP (III) 7D	8.4773144	≈ 3.5
VAE only (IV) 7D	8.1229284	≈ 5.5

TABLE I

MODEL COMPARISON FOR A 2-5-7-DIMENSIONAL LATENT SPACE

Unfortunately, (I) is computationally very expensive, to the point that we could not test it with cross-validation. Early tests did not show a significant improvement w.r.t. the lighter version (II). Thus, we focus our comparison on (II), (III) and (IV). All models were trained in the same manner to avoid training biases: samples were split into overlapping subsequences of size $l_{sub} = 10$, as in [1], and an overlap size equal to $l_{sub} - n_V = 8$, where n_V is the number of standard VAEs. As in [1], the encoder and decoder networks were all made of one hidden layer of 200 units. We implemented a middle layer of 10 hidden units for each frame observed as input in the MLP designed to infer f_t . f_t was composed of 50 basis Gaussian functions, parametrized by standard deviation of 2.5, experimentally chosen following a grid search based on reconstruction error.

For (III), the parameters α , β , τ and dt were experimentally chosen after a grid search based on reconstruction error, with the same constraint as in [1], *i.e.* $\beta = \alpha/4$. We used the values: $\alpha = 2$, $\beta = 0.5$, $\tau = 1/2$ and $dt = 0.5$.

To increase learning speed and stability, we trained all models using a mini-batch of 7, again chosen following a grid search under the constraint of being a multiple of the number of training samples. For all models and for each VAE, we set the number of Monte Carlo samples at $L = 30$ to have a statistically significant sample group, as our batch size was small [19].

For the experiments, we dynamically subsampled our dataset to fit in 70 frames of movements as in [1]. We also normalized the joint angles data between $[-1, 1]$. The whole dataset is uniformly shuffled before each model training to avoid successive overfitting, and thus ensure learning convergence.

VI. RESULTS

We compared the three models based on two metrics: the Mean Squared Error (MSE) between ground truth and reconstruction, and the variance of the reconstruction through time summed on all dimensions and movement samples ($\sum var$). The first one is a precision metric on the reconstruction, while the second is an indicator of the amplitude of reconstructed dynamics. Together, they provide information on the features encoded in the latent space. We averaged these values after the execution of a leave-one-out on sample indices (in the range $[0,9]$) which led to training on 63 samples and testing on 7 samples. These results can be found in Table I.

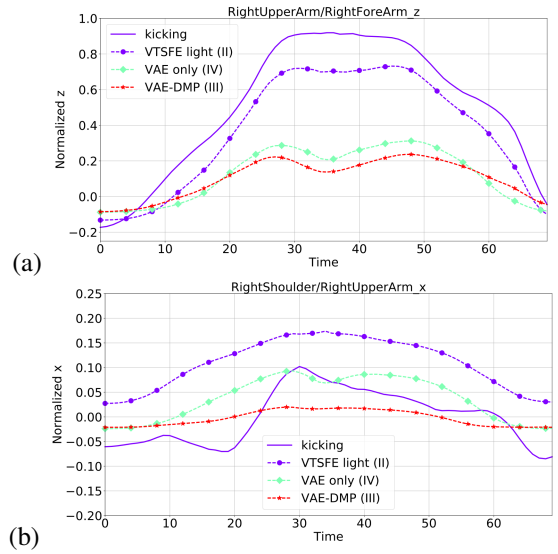


Fig. 3. Reconstruction of a new movement sample from a (a) 2D (b) 7D latent space. The solid line denotes the ground truth curve corresponding to the evolution through time of the normalized (a) z spatial dimension of the right elbow (b) x spatial dimension of the right shoulder angle of the human during a movement of type “kicking”. Dashed lines denote reconstructed data. The purple one corresponds to VTSFE light (II). The red one corresponds to VAE-DMP (III).

Our results show that VTSFE light (II) leads to a slightly lower mean precision of the reconstruction error, despite being almost equivalent to VAE-DMP (III) and (IV), while significantly encoding more dynamics information. This increase in dynamics precision is illustrated in Figure 3a. The reason why (III) and (IV) still reach the best precision is because of static errors of (II) and movement averaging from (III) and (IV), as illustrated in Figure 3b. Also, while precision slightly increases with the number of latent variables for all models (except VAE only), the dynamics encoding is almost constant (except VAE-DMP which decreases in quality).

Finally, the latent space of these models can provide complementary information about encoded dynamics. While the ($\sum var$) indicator accounts for dynamics amplitude, the latent space smoothness accounts for acceleration continuity, which is crucial for prediction. In VAE only (IV) (Figure 4a), trajectories make rough changes in speed and direction. In VAE-DMP (III) (Figure 4b), trajectories are much smoother than VAE only (IV), and better suited for prediction. However, as already observed in the input data space, it lacks information about dynamics amplitude. In VTSFE light (II) (Figure 4c), trajectories are smooth, compatible with prediction and wider than VAE-DMP (III). In particular, it can be observed much more easily in VTSFE light (II) that “bent forward” (purple) and “bent forward strongly” (blue) are similar movement, the second one being an emphasized version of the first one. Table II reports on computation times for 10 training epochs for the 4 models considered in Section V in the same conditions as in Table I, on a 64-bit laptop with 15.5 GB RAM, Intel Core i7-4900MQ CPU @ 2.80 GHz x 8 and NVIDIA Quadro K2100M.

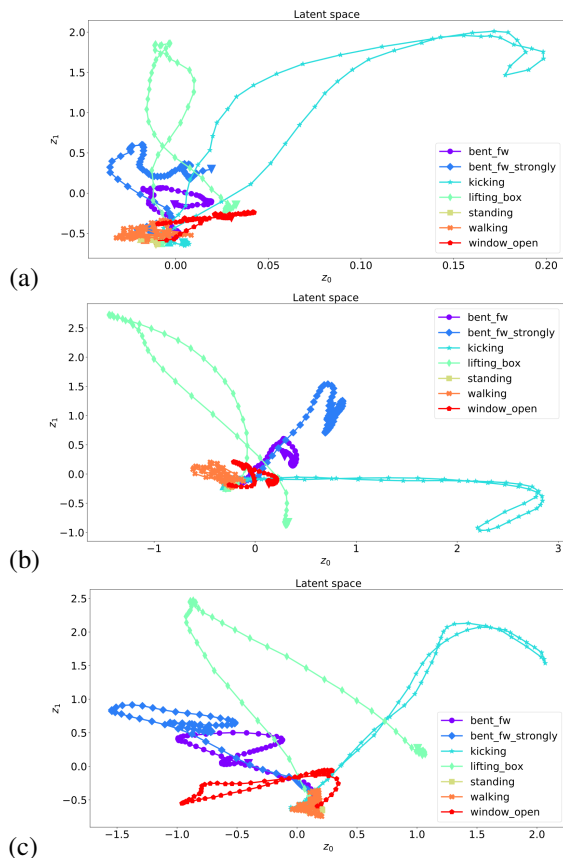


Fig. 4. Latent space of (a) VAE only (IV) (b) VAE-DMP (III) (c) VTSFE light (II) in 2D showing trajectories for a new movement sample for each movement type.

VII. DISCUSSION

However, it could be argued that $\sum var$ isn't a robust indicator and can only suggest the encoded dynamics quality. In fact, while this suggestion matches the one found in latent space about encoded features, these results do not account for a better reconstruction capability in VTSFE than in VAE-DMP or VAE only. Our results strongly suggest a better feature encoding in latent space with VTSFE, i.e. a better encoder, than VAE-DMP or VAE only, but not a better reconstruction, i.e. a better decoder. Thus, it is very likely that a second training phase for VTSFE, in which the encoder weights would be frozen and the loss function would be the one of the classic VAE, would result in a much better reconstruction capability as we would get rid of all encoding constraint in loss function and we would feed the decoder with stable input data, i.e. a constant latent space. But, that is not the scope of this paper which focuses on feature extraction (encoding).

Therefore, our results show that VTSFE (II) seems more suitable than VAE-DMP (III) for prediction and classification of actions based on its inferred latent space from motion capture/wearable sensing data. It is computationally faster, and it encodes a better dynamics of the trajectories, which leads to better reconstruction of high-amplitude joint motions (e.g., as in kicking). The latent space seems more consistent,

	<i>all</i>	<i>separated</i>
VTSFE 2D [$P = 15, L = 15$]	-	killed (> 30 GB RAM)
VTSFE 2D [$P = 5, L = 30$]	-	2h30m
VTSFE 2D [$P = 5, L = 15$]	-	1h30m
VTSFE light 2D [$L = 30$]	9m	9m30s
VAE-DMP 2D [$L = 30$]	12m50 s	16m30s
VAE only 2D, 5D, 7D [$L = 30$]	5m40s	-

TABLE II

COMPUTATION TIMES FOR 10 TRAINING EPOCHS FOR THE DIFFERENT LEARNING SCHEMES.

trajectories in the latent space are smoother, and similar movements are closer (e.g., as in "bent" and "strongly bent").³

VIII. CONCLUSION

In this paper, we presented VTSFE (Variational Time Series Feature Extractor), that can be used to extract relevant features from motion capture/wearable sensing data to recognize and predict the current human activity. We compared it with our open-source implementation of VAE-DMP from [1] and classical VAE, showing that our algorithm is capable of better encoding the dynamics of the captured movements: this is an essential feature for our ongoing work, where VTSFE is needed for predicting the future trajectory of the human motion. Due to Monte Carlo samplings, the computation time for training is still non-negligible, even for our relatively small dataset, which makes it suitable only as a pre-computed model trained offline. Nevertheless, once trained VTSFE is able to encode features online.

In the future, we plan several improvements of our method. In particular, our model is agnostic of the type of input data. While this is a potential advantage (as we could input different types of sensor data), it does not exploit any prior knowledge about the human-body model. We plan to improve the VAE part of our model by testing Ladder Variational Autoencoders [25], which outperform standard VAE in posterior approximation and are used to train a deep architecture of latent layers, and VAE-GAN [26], which outperform VAE by combining it with a Generative Adversarial Network (GAN) that enhances the plausibility of the generated data.

Finally, we would like to make a more thorough⁴ evaluation with a bigger dataset and a varying number of sensors, combining also different input sensors (e.g., IMU, EMG, etc.).

REFERENCES

- [1] N. Chen, M. Karl, and P. Van Der Smagt, "Dynamic movement primitives in latent space of time-dependent variational autoencoders," *16th IEEE-RAS International Conference on Humanoid Robots*, 2016.
- [2] M. Vrigkas, C. Nikou, and I. A. Kakadiaris, "A review of human activity recognition methods," *Front in Rob & AI*, vol. 2, p. 28, 2015.
- [3] A. M. Dollar and H. Herr, "Lower extremity exoskeletons and active orthoses: Challenges and state-of-the-art," *IEEE Transactions on Robotics*, vol. 24, no. 1, pp. 144–158, Feb 2008.

³Our results could be biased by our implementation of VAE-DMP [1], which makes some assumptions about the implementation that were not described in the original paper.

⁴Our evaluation so far has been significantly limited by the availability of a cluster for computations.

- [4] H. A. Varol and M. Goldfarb, "Real-time intent recognition for a powered knee and ankle transfemoral prosthesis," in *ICORR*, June 2007, pp. 16–23.
- [5] G. Ferrer and A. Sanfeliu, "Bayesian human motion intentionality prediction in urban environments," *Pattern Recognition Letters*, vol. 44, pp. 134 – 140, 2014.
- [6] S. Ivaldi, L. Fritzsche, J. Babič, F. Stulp, M. Damsgaard, B. Graimann, G. Belluscio, and F. Nori, "Anticipatory models of human movements and dynamics: the roadmap of the andy project," in *Digital Human Models (DHM)*, 2017.
- [7] S. C. A. . C. Heindl, "Action recognition for human robot interaction in industrial applications," in *IEEE CGVIS*, 2015, pp. 94–99.
- [8] Xsens, "<http://www.xsens.com/products/xsens-mvn/>," 2017.
- [9] P. Evrard and A. Kheddar, "Human-humanoid co-working in a joint table transportation," in *Social Robotics*, G. et al, Ed. Springer, 2012, vol. 7621, pp. 357–366.
- [10] G. Maeda et al, "Probabilistic movement primitives for coordination of multiple human–robot collaborative tasks," *Autonomous Robots*, pp. 1–20, 2016.
- [11] A. Dubois and F. Charpillet, "Human activities recognition with rgb-depth camera using hmm," in *IEEE EMBS*, 2013, pp. 4666–4669.
- [12] C. Mandery, M. Plappert, J. Borrs, and T. Asfour, "Dimensionality reduction for whole-body human motion recognition," in *19th Int Conf on Information Fusion*, July 2016, pp. 355–362.
- [13] K. Fragkiadaki, S. Levine, P. Felsen, and J. Malik, "Recurrent network models for human dynamics," *International Conference on Computer Vision*, 2015.
- [14] D. M. Blei, A. Kucukelbir, and J. D. McAuliffe, "Variational inference: A review for statisticians," *eprint arXiv:1601.00670*, 2016.
- [15] S. Schaal, "Dynamic movement primitives-a framework for motor control in humans and humanoid robotics," in *Adaptive motion of animals and machines*. Springer, 2006, pp. 261–280.
- [16] J. Bütepage, M. Black, D. Kragic, and H. Kjellström, "Deep representation learning for human motion prediction and classification," *arXiv preprint arXiv:1702.07486*, 2017.
- [17] J. Martinez, M. J. Black, and J. Romero, "On human motion prediction using recurrent neural networks," *CVPR*, 2017.
- [18] J. Chung, K. Kastner, L. Dinh, K. Goel, A. Courville, and Y. Bengio, "A recurrent latent variable model for sequential data," *NIPS*, 2015.
- [19] D. P. Kingma and M. Welling, "Auto-encoding variational bayes," *Int Conf on Learning Representations (ICLR)*, 2014.
- [20] M. Karl, M. Soelch, J. Bayer, and P. Van Der Smagt, "Deep variational bayes filters: Unsupervised learning of state space models from raw data," *Int Conf on Learning Representations (ICLR)*, 2017.
- [21] J. Duchi, "Derivations for linear algebra and optimization." [Online]. Available: http://web.stanford.edu/~jduchi/projects/general_notes.pdf
- [22] C. Djork-Arn, T. Unterthiner, and S. Hochreiter, "Fast and accurate deep network learning by exponential linear units (elus)," *The International Conference on Learning Representations (ICLR)*, 2016.
- [23] D. P. Kingma and J. Lei Ba, "Adam : A method for stochastic optimization," *Int Conf on Learning Representations (ICLR)*, 2015.
- [24] J. Duchi, E. Hazan, and Y. Singer, "Adaptive subgradient methods for online learning and stochastic optimization," *Journal of Machine Learning Research* 12, 2011.
- [25] C. K. Sø nderby, T. Raiko, L. Maalø e, S. r. K. Sø nderby, and O. Winther, "Ladder variational autoencoders," *arXiv preprint arXiv:1602.02282*, 2016.
- [26] A. B. L. Larsen, S. r. K. Sø nderby, H. Larochelle, and O. Winther, "Autoencoding beyond pixels using a learned similarity metric," *arXiv preprint arXiv:1512.09300*, 2016.

APPENDIX I
RELATED WORKS

A. VAE

$$\begin{aligned} \ln(p_\theta([x_k]_{k=1}^K)) &= \ln\left(\prod_{k=1}^K p_\theta(x_k)\right) \\ &= \sum_{k=1}^K \ln(p_\theta(x_k)) \end{aligned} \quad (20)$$

$$\begin{aligned} \ln(p_\theta(x_k)) &= \int_z q_\phi(z|x_k) \ln(p_\theta(x_k)) dz \\ &= \int_z q_\phi(z|x_k) \ln\left(\frac{p_\theta(z, x_k)}{q_\phi(z|x_k)}\right) + q_\phi(z|x_k) \ln\left(\frac{q_\phi(z|x_k)}{p_\theta(z|x_k)}\right) dz \\ &= ELBO + D_{KL}(q_\phi(z|x_k) \parallel p_\theta(z|x_k)) \end{aligned} \quad (21)$$

where *ELBO* is the Evidence Lower Bound.

$$\begin{aligned} -ELBO &= -\int_z q_\phi(z|x_k) \ln\left(\frac{p_\theta(z, x_k)}{q_\phi(z|x_k)}\right) dz \\ &= -\int_z q_\phi(z|x_k) \ln(p_\theta(x_k|z)) + q_\phi(z|x_k) \ln\left(\frac{p_\theta(z)}{q_\phi(z|x_k)}\right) dz \\ &= -\mathbb{E}_{q_\phi(z|x_k)}[\ln(p_\theta(x_k|z))] + D_{KL}(q_\phi(z|x_k) \parallel p_\theta(z)) \end{aligned} \quad (22)$$

B. DVBF

$$\begin{aligned} p_\theta(x_{1:T}|u_{1:T}, z_1) &= \int_{z_{2:T}} p_\theta(x_{1:T}|z_{1:T}, u_{1:T}) p_\theta(z_{2:T}|u_{1:T}) dz_{2:T} \\ &= \int_{z_{2:T}} \int_{\beta_{1:T}} p_\theta(x_{1:T}|z_{1:T}, u_{1:T}) p_\theta(z_{2:T}|\beta_{1:T}, u_{1:T}) p_\theta(\beta_{1:T}) d\beta_{1:T} dz_{2:T} \\ &= \int_{z_{2:T}} \int_{\beta_{1:T}} p_\theta(\beta_{1:T}) \prod_{t=1}^T p_\theta(x_t|z_t) \prod_{t=2}^T p_\theta(z_t|z_{t-1}, u_{t-1}, \beta_{t-1}) d\beta_{1:T} dz_{2:T} \end{aligned} \quad (23)$$

Given the deterministic transition (4), they noticed that $\prod_{t=2}^T p_\theta(z_t|z_{t-1}, u_{t-1}, \beta_{t-1})$ was a product of Dirac distributions and thus:

$$p_\theta(x_{1:T}|u_{1:T}, z_1) = \int_{\beta_{1:T}} p_\theta(\beta_{1:T}) p_\theta(x_t|z_1) \prod_{t=2}^T p_\theta(x_t|\hat{z}_t) d\beta_{1:T} \quad (24)$$

where $\hat{z}_t = g(z_{t-1}, u_{t-1}, \beta_{t-1})$.

$$\begin{aligned} &\ln(p_\theta(x_{1:T}|u_{1:T}, z_1)) \\ &= \ln\left(\int_{\beta_{1:T}} \frac{q_\phi(\beta_{1:T}|x_{1:T}, u_{1:T}, z_1, \hat{z}_{2:T})}{q_\phi(\beta_{1:T}|x_{1:T}, u_{1:T}, z_1, \hat{z}_{2:T})} p_\theta(\beta_{1:T}) p_\theta(x_t|z_1) \prod_{t=2}^T p_\theta(x_t|\hat{z}_t) d\beta_{1:T}\right) \\ &\geq \int_{\beta_{1:T}} q_\phi(\beta_{1:T}|x_{1:T}, u_{1:T}, z_1, \hat{z}_{2:T}) \ln\left(\frac{p_\theta(\beta_{1:T})}{q_\phi(\beta_{1:T}|x_{1:T}, u_{1:T}, z_1, \hat{z}_{2:T})} p_\theta(x_t|z_1) \prod_{t=2}^T p_\theta(x_t|\hat{z}_t)\right) d\beta_{1:T} = LB \end{aligned} \quad (25)$$

where:

$$LB = \mathbb{E}_{q_\phi(\beta_{1:T}|x_{1:T}, u_{1:T}, z_1, \hat{z}_{2:T})} \left[\ln \left(p_\theta(x_t|z_1) \prod_{t=2}^T p_\theta(x_t|\hat{z}_t) \right) \right] - D_{KL}(q_\phi(\beta_{1:T}|x_{1:T}, u_{1:T}, z_1, \hat{z}_{2:T}) \parallel p_\theta(\beta_{1:T})) \quad (26)$$

APPENDIX II METHODS

A. Our improvements to VAE-DMP

1) Tighter lower bound:

$$\begin{aligned} q_\phi(z_{1:T}|x_{1:T}) &= \frac{q_\phi(z_{1:T}, x_{1:T})}{q_\phi(x_{1:T})} \\ &= \prod_{t \in \{1, 2, T\}} q_\phi(z_t|x_t) \prod_{t=3}^{T-1} q_\phi(z_t|x_{1:T}, z_{t-1}, z_{t-2}, z_T) \end{aligned} \quad (27)$$

Given $\forall t \in [3, T-1]$, $z_t = g(z_{t-1}, z_{t-2}, z_T, \epsilon_t, f_t)$, where g is a deterministic transition function, we can push (27) a little further :

$$\begin{aligned} &q_\phi(z_{1:T}|x_{1:T}) \\ &= \prod_{t \in \{1, 2, T\}} q_\phi(z_t|x_t) \prod_{t=2}^{T-2} q_\phi(g(z_t, z_{t-1}, z_T, \epsilon_t, f_t)|x_{1:T}, z_t, z_{t-1}, z_T) \\ &= \prod_{t \in \{1, 2, T\}} q_\phi(z_t|x_t) \prod_{t=2}^{T-2} q_\phi(\epsilon_t, f_t|x_{1:T}, z_t, z_{t-1}, z_T) \\ &= \prod_{t \in \{1, 2, T\}} q_\phi(z_t|x_t) \prod_{t=2}^{T-2} \frac{q_\phi(\epsilon_t, f_t, x_{1:T}, z_t, z_{t-1}, z_T)}{q_\phi(x_{1:T}, z_t, z_{t-1}, z_T)} \\ &= \prod_{t \in \{1, 2, T\}} q_\phi(z_t|x_t) \prod_{t=2}^{T-2} \frac{q_\phi(f_t|x_{1:T})q_\phi(\epsilon_t|f_t, x_{t+1}, z_t, z_{t-1}, z_T)q_\phi(x_{1:T}, z_t, z_{t-1}, z_T)}{q_\phi(x_{1:T}, z_t, z_{t-1}, z_T)} \\ &= \prod_{t \in \{1, 2, T\}} q_\phi(z_t|x_t) \prod_{t=2}^{T-2} q_\phi(\epsilon_t|f_t, x_{t+1}, z_t, z_{t-1}, z_T)q_\phi(f_t|x_{1:T}) \end{aligned} \quad (28)$$

In the same way:

$$\begin{aligned} p_\theta(z_{1:T}) &= \prod_{t \in \{1, 2, T\}} p_\theta(z_t) \prod_{t=3}^{T-1} p_\theta(z_t|z_{t-1}, z_{t-2}, z_T) \\ &= \prod_{t \in \{1, 2, T\}} p_\theta(z_t) \prod_{t=2}^{T-2} p_\theta(\epsilon_t, f_t|z_t, z_{t-1}, z_T) \\ &= \prod_{t \in \{1, 2, T\}} p_\theta(z_t) \prod_{t=2}^{T-2} p_\theta(\epsilon_t)p_\theta(f_t) \end{aligned} \quad (29)$$

And finally:

$$p_\theta(x_{1:T}|z_{1:T}) = \prod_{t=1}^T p_\theta(x_t|z_t) \quad (30)$$

(27) and (30) lead to:

$$\begin{aligned}
& \mathbb{E}_{q_\phi(z_{1:T}|x_{1:T})}[\ln(p_\theta(x_{1:T}|z_{1:T}))] \\
&= \mathbb{E}_{q_\phi(z_{1:T}|x_{1:T})} \left[\sum_{t=1}^T \ln(p_\theta(x_t|z_t)) \right] \\
&= \sum_{t_1=1}^T \int_{z_{1:T}} \prod_{t_2 \in \{1,2,T\}} q_\phi(z_{t_2}|x_{t_2}) \prod_{t_2=3}^{T-1} q_\phi(z_{t_2}|x_{1:T}, z_{t_2-1}, z_{t_2-2}, z_T) \ln(p_\theta(x_{t_1}|z_{t_1})) dz_{1:T} \\
&= \sum_{t_1 \in \{1,2,T\}} \left[\int_{z_{t_1}} q_\phi(z_{t_1}|x_{t_1}) \ln(p_\theta(x_{t_1}|z_{t_1})) \right. \\
&\quad \times \left[\int_{z_{[1:T] \setminus \{t_1\}}} \prod_{t_2 \in \{1,2,T\} \setminus \{t_1\}} q_\phi(z_{t_2}|x_{t_2}) \right. \\
&\quad \times \left. \left. \prod_{t_2=3}^{T-1} q_\phi(z_{t_2}|x_{1:T}, z_{t_2-1}, z_{t_2-2}, z_T) dz_{[1:T] \setminus \{t_1\}} \right] dz_{t_1} \right] \\
&+ \sum_{t_1=3}^{T-1} \left[\int_{z_{1:t_1}, z_T} \prod_{t_2 \in \{1,2,T\}} q_\phi(z_{t_2}|x_{t_2}) \prod_{t_2=3}^{t_1} q_\phi(z_{t_2}|x_{1:T}, z_{t_2-1}, z_{t_2-2}, z_T) \ln(p_\theta(x_{t_1}|z_{t_1})) \right. \\
&\quad \times \left. \left[\int_{z_{[t_1+1:T-1]}} \prod_{t_2=t_1+1}^{T-1} q_\phi(z_{t_2}|x_{1:T}, z_{t_2-1}, z_{t_2-2}, z_T) dz_{[t_1+1:T-1]} \right] dz_{1:t_1} dz_T \right] \\
&= \sum_{t \in \{1,2,T\}} \left[\int_{z_t} q_\phi(z_t|x_t) \ln(p_\theta(x_t|z_t)) dz_t \right] \\
&+ \sum_{t=3}^{T-1} \left[\int_{z_{1:t}, z_T} q_\phi(z_{1:t}, z_T|x_{1:T}) \ln(p_\theta(x_t|z_t)) dz_{1:t} dz_T \right] \\
&= \sum_{t \in \{1,2,T\}} \mathbb{E}_{q_\phi(z_t|x_t)}[\ln(p_\theta(x_t|z_t))] + \sum_{t=3}^{T-1} \mathbb{E}_{q_\phi(z_{1:t}, z_T|x_{1:T})}[\ln(p_\theta(x_t|z_t))]
\end{aligned} \tag{31}$$

Besides, (29) and (28) lead to:

$$\begin{aligned}
& D_{KL}(q_\phi(z_{1:T}|x_{1:T}) \parallel p_\theta(z_{1:T})) \\
&= \int_{z_{1:T}} q_\phi(z_{1:T}|x_{1:T}) \ln \left(\frac{q_\phi(z_{1:T}|x_{1:T})}{p_\theta(z_{1:T})} \right) dz_{1:T} \\
&= \int_{z_{1:T}} q_\phi(z_{1:T}|x_{1:T}) \ln \left(\frac{\prod_{t \in \{1,2,T\}} q_\phi(z_t|x_t) \prod_{t=2}^{T-2} q_\phi(\epsilon_t|f_t, x_{t+1}, z_t, z_{t-1}, z_T) q_\phi(f_t|x_{1:T})}{\prod_{t \in \{1,2,T\}} p_\theta(z_t) \prod_{t=2}^{T-2} p_\theta(\epsilon_t) p_\theta(f_t)} \right) dz_{1:T} \\
&= \int_{z_{1:T}} q_\phi(z_{1:T}|x_{1:T}) \left[\sum_{t \in \{1,2,T\}} \ln \left(\frac{q_\phi(z_t|x_t)}{p_\theta(z_t)} \right) + \sum_{t=2}^{T-2} \ln \left(\frac{q_\phi(\epsilon_t|f_t, x_{t+1}, z_t, z_{t-1}, z_T)}{p_\theta(\epsilon_t)} \right) \right. \\
&\quad \left. + \sum_{t=2}^{T-2} \ln(q_\phi(f_t|x_{1:T})) - \sum_{t=2}^{T-2} \ln(p_\theta(f_t)) \right] dz_{1:T} \\
&= \sum_{t \in \{1,2,T\}} \int_{z_t} q_\phi(z_t|x_t) \ln \left(\frac{q_\phi(z_t|x_t)}{p_\theta(z_t)} \right) dz_t \\
&\quad + \sum_{t_1=2}^{T-2} \left[\int_{z_{1:t_1}, z_T} \int_{\epsilon_{t_1}} \int_{f_{t_1}} \prod_{t_2 \in \{1,2,T\}} q_\phi(z_{t_2}|x_{t_2}) \prod_{t_2=3}^{t_1} q_\phi(z_{t_2}|x_{1:T}, z_{t_2-1}, z_{t_2-2}, z_{goal}) \right. \\
&\quad \times q_\phi(\epsilon_{t_1}|f_{t_1}, x_{t_1+1}, z_{t_1}, z_{t_1-1}, z_T) q_\phi(f_{t_1}|x_{1:T}) \left[\ln \left(\frac{q_\phi(\epsilon_{t_1}|f_{t_1}, x_{t_1+1}, z_{t_1}, z_{t_1-1}, z_T)}{p_\theta(\epsilon_{t_1})} \right) \right. \\
&\quad \left. \left. + \ln(q_\phi(f_{t_1}|x_{1:T})) - \ln(p_\theta(f_{t_1})) \right) \right] \\
&\quad \times \left[\int_{z_{[t_1+1:T-1]}} \prod_{t_2=t_1+1}^{T-1} q_\phi(z_{t_2}|x_{1:T}, z_{t_2-1}, z_{t_2-2}, z_{goal}) dz_{[t_1+1:T-1]} \right] df_{t_1} d\epsilon_{t_1} dz_{1:t_1} dz_T \\
&= \sum_{t \in \{1,2,T\}} D_{KL}(q_\phi(z_t|x_t) \parallel p_\theta(z_t)) \\
&\quad + \sum_{t_1=2}^{T-2} \mathbb{E}_{q_\phi(z_{1:t_1}, z_T|x_{1:T})} \left[\int_{f_{t_1}} q_\phi(f_{t_1}|x_{1:T}) \right. \\
&\quad \left[\int_{\epsilon_{t_1}} q_\phi(\epsilon_{t_1}|f_{t_1}, x_{t_1+1}, z_{t_1}, z_{t_1-1}, z_T) \ln \left(\frac{q_\phi(\epsilon_{t_1}|f_{t_1}, x_{t_1+1}, z_{t_1}, z_{t_1-1}, z_T)}{p_\theta(\epsilon_{t_1})} \right) d\epsilon_{t_1} \right. \\
&\quad \left. + \ln(q_\phi(f_{t_1}|x_{1:T})) \int_{\epsilon_{t_1}} q_\phi(\epsilon_{t_1}|f_{t_1}, x_{t_1+1}, z_{t_1}, z_{t_1-1}, z_T) d\epsilon_{t_1} \right. \\
&\quad \left. \left. - \ln(p_\theta(f_{t_1})) \int_{\epsilon_{t_1}} q_\phi(\epsilon_{t_1}|f_{t_1}, x_{t_1+1}, z_{t_1}, z_{t_1-1}, z_T) d\epsilon_{t_1} \right] df_{t_1} \right]
\end{aligned} \tag{32}$$

As f_t is inferred deterministically by $x_{1:T}$, the probability of f_t given $x_{1:T}$ equals 1. Thus, the distribution $q_\phi(f_t|x_{1:T})$ is a Dirac function centered at \hat{f}_t , where \hat{f}_t is the inferred value of f_t for a given $x_{1:T}$. Therefore, $\int_{f_{t_1}} q_\phi(f_{t_1}|x_{1:T}) \ln(q_\phi(f_{t_1}|x_{1:T})) df_{t_1} = \ln(1) = 0$ and $\int_{f_{t_1}} q_\phi(f_{t_1}|x_{1:T}) \ln(p_\theta(f_{t_1})) df_{t_1} = \ln(p_\theta(\hat{f}_t))$. Thereby, (32)

simplifies as following:

$$\begin{aligned}
& D_{KL}(q_\phi(z_{1:T}|x_{1:T}) \parallel p_\theta(z_{1:T})) \\
&= \sum_{t \in \{1,2,T\}} D_{KL}(q_\phi(z_t|x_t) \parallel p_\theta(z_t)) \\
&\quad + \sum_{t_1=2}^{T-2} \mathbb{E}_{q_\phi(z_{1:t_1}, z_T|x_{1:T})} \left[-\ln(p_\theta(\hat{f}_{t_1})) \right. \\
&\quad \quad \left. + \int_{\epsilon_{t_1}} q_\phi(\epsilon_{t_1}|\hat{f}_{t_1}, x_{t_1+1}, z_{t_1}, z_{t_1-1}, z_T) \ln \left(\frac{q_\phi(\epsilon_{t_1}|\hat{f}_{t_1}, x_{t_1+1}, z_{t_1}, z_{t_1-1}, z_T)}{p_\theta(\epsilon_{t_1})} \right) d\epsilon_{t_1} \right] \quad (33) \\
&= \sum_{t \in \{1,2,T\}} D_{KL}(q_\phi(z_t|x_t) \parallel p_\theta(z_t)) \\
&\quad + \sum_{t=2}^{T-2} \mathbb{E}_{q_\phi(z_{1:t}, z_T|x_{1:T})} \left[-\ln(p_\theta(\hat{f}_t)) \right. \\
&\quad \quad \left. + D_{KL}(q_\phi(\epsilon_t|\hat{f}_t, x_{t+1}, z_t, z_{t-1}, z_T) \parallel p_\theta(\epsilon_t)) \right]
\end{aligned}$$

Light version calculation of $D_{KL}(q_\phi(\epsilon_t|f_t, x_{t+1}, z_t, z_{t-1}, z_T) \parallel p_\theta(\epsilon_t))$:

$$\begin{aligned}
& D_{KL}(q_\phi(\epsilon_t|f_t, x_{t+1}, z_t, z_{t-1}, z_T) \parallel p_\theta(\epsilon_t)) \\
&= \frac{1}{2} \left[\ln \left(\frac{|\sigma_{scale}^2 I|}{|\sigma_{scale}^2 I \sigma_{\epsilon,t}^2 I|} \right) - d_z + \text{tr} \left((\sigma_{scale}^2 I)^{-1} \sigma_{scale}^2 I \sigma_{\epsilon,t}^2 I \right) + (-\sigma_{scale} \odot \mu_{\epsilon,t}) (\sigma_{scale}^2 I)^{-1} (-\sigma_{scale} \odot \mu_{\epsilon,t})^T \right] \quad (34) \\
&= \frac{1}{2} \sum_{i=1}^{d_z} [-\ln(\sigma_{\epsilon,t,i}^2) - 1 + \sigma_{\epsilon,t,i}^2 + \mu_{\epsilon,t,i}^2]
\end{aligned}$$

The final *ELBO* is thus defined as following :

$$\begin{aligned}
ELBO &= \mathbb{E}_{q_\phi(z_{1:T}|x_{1:T})}[\ln(p_\theta(x_{1:T}|z_{1:T}))] - D_{KL}(q_\phi(z_{1:T}|x_{1:T}) \parallel p_\theta(z_{1:T})) \\
&\leq \left(\sum_{t \in \{1,2,T\}} \mathbb{E}_{q_\phi(z_t|x_t)}[\ln(p_\theta(x_t|z_t))] \right. \\
&\quad + \sum_{t=3}^{T-1} \left[\mathbb{E}_{q_\phi(z_{1:t}, z_T|x_{1:T})}[\ln(p_\theta(x_t|z_t))] \right. \\
&\quad \left. \left. + \mathbb{E}_{q_\phi(z_{1:T}|x_{1:T})}[\ln(p_\theta(\hat{f}_{t-1}|z_{1:T}))] \right] \right) \\
&\quad - \left(\sum_{t \in \{1,2,T\}} D_{KL}(q_\phi(z_t|x_t) \parallel p_\theta(z_t)) \right. \\
&\quad \left. + \sum_{t=2}^{T-2} \mathbb{E}_{q_\phi(z_{1:t}, z_T|x_{1:T})} \left[D_{KL}(q_\phi(\epsilon_t|\hat{f}_t, x_{t+1}, z_t, z_{t-1}, z_T) \parallel p_\theta(\epsilon_t)) \right] \right) \\
&\leq \left(\sum_{t \in \{1,2,T\}} \mathbb{E}_{q_\phi(z_t|x_t)}[\ln(p_\theta(x_t|z_t))] \right. \\
&\quad + \sum_{t=3}^{T-1} \mathbb{E}_{q_\phi(z_{1:t}, z_T|x_{1:T})}[\ln(p_\theta(x_t|z_t))] \\
&\quad - \left(\sum_{t \in \{1,2,T\}} D_{KL}(q_\phi(z_t|x_t) \parallel p_\theta(z_t)) \right. \\
&\quad \left. + \sum_{t=2}^{T-2} \mathbb{E}_{q_\phi(z_{1:t}, z_T|x_{1:T})} \left[D_{KL}(q_\phi(\epsilon_t|\hat{f}_t, x_{t+1}, z_t, z_{t-1}, z_T) \parallel p_\theta(\epsilon_t)) \right] \right) \\
&\approx \left(\sum_{t=1}^T \mathbb{E}_{q_\phi(z_t|x_t)}[\ln(p_\theta(x_t|z_t))] \right) \\
&\quad - \left(\sum_{t \in \{1,2,T\}} D_{KL}(q_\phi(z_t|x_t) \parallel p_\theta(z_t)) \right. \\
&\quad \left. + \sum_{t=3}^{T-1} D_{KL}(q_\phi(\epsilon_t|\hat{f}_t, x_{t+1}, z_t, z_{t-1}, z_T) \parallel p_\theta(\epsilon_t)) \right)
\end{aligned} \tag{35}$$

where the latter expression is equivalent to the lower bound of VAE-DMP.